



This is the accepted manuscript made available via CHORUS. The article has been published as:

## Ultrafast X-Ray Scattering Reveals Composite Amplitude Collective Mode in the Weyl Charge Density Wave Material

$$\left( \text{TaSe} \right)_{4/3} \text{I}$$

Quynh L. Nguyen et al.

Phys. Rev. Lett. **131**, 076901 — Published 14 August 2023

DOI: [10.1103/PhysRevLett.131.076901](https://doi.org/10.1103/PhysRevLett.131.076901)

# Ultrafast x-ray scattering reveals composite amplitude collective mode in the Weyl charge density wave material $(\text{TaSe}_4)_2\text{I}$

Quynh L. Nguyen,<sup>1,2,\*</sup> Ryan A. Duncan,<sup>1,2,\*</sup> Gal Orenstein,<sup>1,2</sup> Yijing Huang,<sup>1,2,3</sup> Viktor Krapivin,<sup>1,2,3</sup> Gilberto de la Peña,<sup>1,2</sup> Chance Ornelas-Skarin,<sup>1,2,3</sup> David A. Reis,<sup>1,2,3,4</sup> Peter Abbamonte,<sup>5</sup> Simon Bettler,<sup>5,6</sup> Matthieu Chollet,<sup>7</sup> Matthias C. Hoffmann,<sup>7</sup> Matthew Hurley,<sup>8</sup> Soyeun Kim,<sup>5,6</sup> Patrick S. Kirchmann,<sup>2</sup> Yuya Kubota,<sup>9</sup> Fahad Mahmood,<sup>5,6</sup> Alexander Miller,<sup>8</sup> Taito Osaka,<sup>9</sup> Kejian Qu,<sup>5,6</sup> Takahiro Sato,<sup>7</sup> Daniel P. Shoemaker,<sup>6,10</sup> Nicholas Sirica,<sup>11</sup> Sanghoon Song,<sup>7</sup> Jade Stanton,<sup>8</sup> Samuel W. Teitelbaum,<sup>8</sup> Sean E. Tilton,<sup>8</sup> Tadashi Togashi,<sup>9,12</sup> Diling Zhu,<sup>7</sup> and Mariano Trigo<sup>1,2</sup>

<sup>1</sup>*Stanford PULSE Institute, SLAC National Accelerator Laboratory, Menlo Park, California, 94025, United States*

<sup>2</sup>*Stanford Institute for Materials and Energy Sciences,*

*SLAC National Accelerator Laboratory, Menlo Park, California, 94025, United States*

<sup>3</sup>*Department of Applied Physics, Stanford University, Stanford, California, 94305, United States*

<sup>4</sup>*Department of Photon Science, Stanford University, Stanford, California, 94305, United States*

<sup>5</sup>*Department of Physics, University of Illinois at Urbana-Champaign, Urbana, Illinois, 61801, United States*

<sup>6</sup>*Materials Research Laboratory, University of Illinois at Urbana-Champaign, Urbana, Illinois, 61801, United States*

<sup>7</sup>*Linac Coherent Light Source, SLAC National Accelerator Laboratory, Menlo Park, California, 94025, United States*

<sup>8</sup>*Department of Physics, Arizona State University, Tempe, Arizona, 85281, United States*

<sup>9</sup>*RIKEN SPring-8 Center, 1-1-1 Kouto, Sayo-cho, Sayo-gun, Hyogo 679-5148, Japan*

<sup>10</sup>*Department of Materials Science and Engineering,*

*University of Illinois at Urbana-Champaign, Urbana, Illinois, 61801, United States*

<sup>11</sup>*Center for Integrated Nanotechnologies, Los Alamos National Laboratory, Los Alamos, New Mexico, 87545, United States*

<sup>12</sup>*Japan Synchrotron Radiation Research Institute,*

*1-1-1 Kouto, Sayo-cho, Sayo-gun, Hyogo 679-5198, Japan*

(Dated: July 19, 2023)

We report ultrafast x-ray scattering experiments of the quasi-1D charge density wave (CDW) material  $(\text{TaSe}_4)_2\text{I}$  following ultrafast infrared photoexcitation. From the time-dependent diffraction signal at the CDW sidebands we identify a 0.11 THz amplitude mode derived primarily from a transverse acoustic mode of the high-symmetry structure. From our measurements we determine that this mode interacts with the valence charge indirectly through another collective mode, and that the CDW system in TSI has a composite nature supporting multiple dynamically active structural degrees of freedom.

Charge density wave (CDW) materials are low dimensional systems that exhibit spontaneously broken symmetries associated with instabilities in the Fermi surface. These systems are characterized by a modulation of the valence electron density and a corresponding lattice distortion due to the electron-lattice interaction [1, 2]. When only a single lattice component is involved in the instability, the equilibrium distortion coincides with the CDW amplitude mode. However, in the composite case, i.e. where more than one lattice mode are involved, the observed equilibrium distortion alone does not contain enough information to identify the active degrees of freedom of the CDW system.

In materials where the CDW is composed of multiple degrees of freedom, understanding the ground state and excitations requires a probe able to disentangle these interacting modes. Time-domain scattering techniques [3] can provide a direct probe of these couplings by perturbing and observing the dynamics of different interacting modes. Surprisingly, most works on ultrafast spectroscopy of prototypical CDW materials can be under-

stood in terms of a single order parameter and a single active coordinate [4–8]. Here we use an x-ray free electron laser (XFEL) to study the collective modes of the quasi-1D CDW material  $(\text{TaSe}_4)_2\text{I}$  (TSI) after ultrafast near-infrared excitation. We observe an amplitude mode of acoustic character with a frequency of 0.11 THz, which is below the frequency of the recently observed massive phase mode in this material [9]. We find that the canonical treatment of CDWs based on a single lattice coordinate is insufficient to explain the observed behavior, revealing the composite nature of the order parameter. These results highlight the power of ultrafast spectroscopy to disentangle coupled degrees of freedom in condensed matter.

TSI is a chiral quasi-1D Weyl semimetal with a crystal structure in the I422 space group dominated by parallel  $(\text{TaSe}_4)_n$  chains extending along the  $c$ -axis. Upon cooling below a temperature of  $T_c = 163$  K it exhibits a transition into a CDW phase [10]. As a Weyl-CDW material it has attracted recent interest [11–14] due to its potential for realizing a so-called dynamical axion insulator state [15], a correlated topological phase where the phase mode of the CDW becomes an analogue of the proposed axial field in high energy physics [16, 17]. Neutron [18] and x-ray diffraction [19, 20] studies indicate that the CDW distur-

---

\* These authors contributed equally to this work.

tion projects primarily onto the transverse acoustic (TA) mode (with a magnitude of  $0.13 \text{ \AA}$ ) and onto two optical modes with  $B_1$  and  $B_2$  symmetry (with a magnitude of  $0.03 \text{ \AA}$ ). These optical modes yield a tetramerization of the tantalum atoms along the chain direction [20]. This distortion occurs with a small but finite wavevector  $\mathbf{q}_{\text{CDW}} = (\alpha \alpha \beta)$ , where  $\alpha \approx 0.05$  and  $\beta \approx 0.1$  reciprocal lattice units (r.l.u.). Band theory considerations [21] and *ab initio* density functional theory calculations [22] predict an instability of the I422 phase to a tetramerization of the Ta atoms along the chain similar to the secondary projection of the CDW lattice distortion mentioned above. To explain the nonzero wavevector of the CDW it was speculated that the CDW instability is driven by the soft optical Ta-tetramerization mode, which also couples to the strain and leads to an actual CDW distortion of mixed acoustic-optical character [18]. However, because these mixed modes gradually renormalize with temperature, it is not possible to experimentally distinguish a composite order parameter from a one-dimensional distortion along a single lattice mode using temperature-dependent equilibrium measurements alone. On the other hand, ultrafast excitation can induce nonequilibrium dynamics which reflect the mode composition of the CDW order. The collective modes of the CDW in TSI are as yet poorly understood and highly unconventional, as highlighted by the recent observation of an exotic massive phason [9]. In our time- and momentum-resolved measurements we identify an amplitude mode of the CDW and determine that it derives from an acoustic mode of the undistorted phase. From the observed dynamics we determine that the excitation of this mode must be mediated through another structural degree of freedom, likely associated with Ta tetramerization. In this sense, TSI is an example of a complex CDW system where the dynamics do not conform to the conventional scenario based on a single degree of freedom [4–8].

The TSI crystals were grown by chemical vapor transport of the elements in a thermal gradient of  $600 \text{ }^\circ\text{C}$  to  $500 \text{ }^\circ\text{C}$ , as described in Refs. [23, 24]. The ultrafast x-ray scattering experiments were performed at the XPP instrument of the Linac Coherent Light Source (LCLS) [25, 26] at the SLAC National Accelerator Laboratory and at the BL3 hutch of the SPring-8 Angstrom Compact free-electron LAser (SACLA) [27] at the RIKEN SPring-8 Center. A schematic of the experimental configuration is shown in Fig. 1(a). In the experiments at LCLS (SACLA) a  $2 \text{ }\mu\text{m}$  (800 nm) infrared laser pulse with a duration of  $\sim 50 \text{ fs}$  (45 fs) was used to excite the TSI sample with a  $(1\ 1\ 0)$  surface normal at an incidence angle of  $7^\circ$  from the sample surface. The sample was probed with a  $\sim 30 \text{ fs}$  ( $< 10 \text{ fs}$ ) x-ray pulse, and the diffraction patterns were recorded on a 2D array detector positioned 600 mm (620 mm) away from the sample. The x-ray photon energy and bandwidth were 9.55 keV and 0.5 eV respectively, and the timing jitter between the pump and probe pulses was corrected on a single-shot basis to achieve a time resolution of  $< 80 \text{ fs}$  [28, 29].

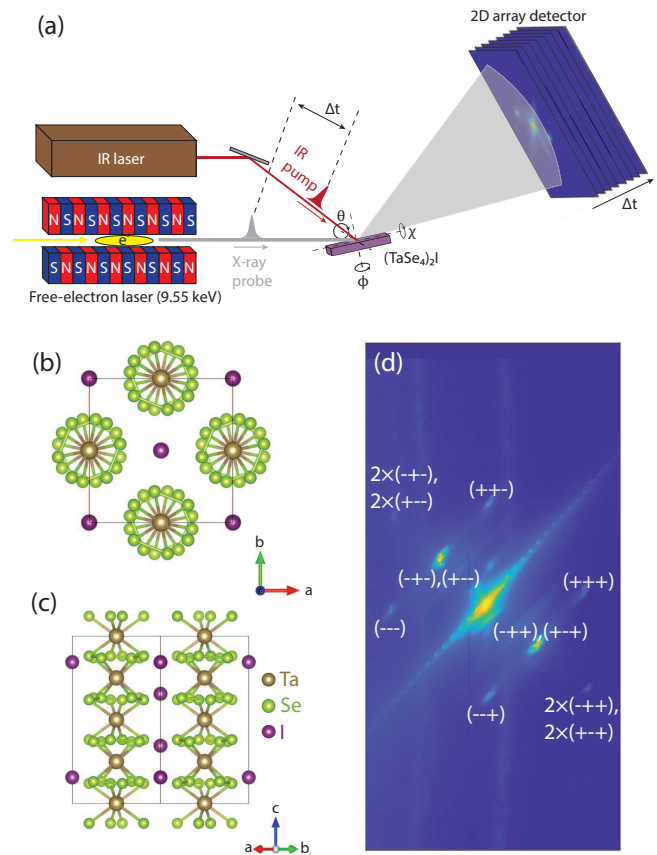


FIG. 1. (a) Schematic of the experimental setup. (b,c) Conventional unit cell of TSI in the high-temperature (I422) phase. The lattice constants are  $a, b = 9.5317 \text{ \AA}$  and  $c = 12.761 \text{ \AA}$ . (d) Integrated diffraction image of a scan of the sample azimuth  $\phi$  around the  $(2\ 2\ 4)$  Bragg peak in the CDW phase. Several first- and second-order sidebands are visible. The discrete spots passing diagonally through the Bragg peak are the intersections of the Bragg rod with the Ewald sphere as  $\phi$  is varied.

The pump pulses were focused to a spot on the sample with area of  $0.15 \times 1.2 \text{ mm}^2$ . The x-rays were incident at grazing angles between  $0.5^\circ$ – $1^\circ$  with respect to the sample surface in order to match the x-ray and optical penetration depths, and the x-ray spot sizes on the sample were  $0.1 \times 1.2 \text{ mm}^2$  ( $0.03 \times 2.6 \text{ mm}^2$ ). The sample temperature was maintained at  $\sim 150 \text{ K}$  using a cryostream cooling system. We do not observe a pump wavelength dependence of the response.

Fig. 1(d) shows the sum of the detector images obtained by scanning the sample azimuthal angle  $\phi$  (i.e., the angle parametrizing rotations about the sample normal) near the  $(2\ 2\ 4)$  crystal Bragg reflection. Several sidebands corresponding to the CDW lattice distortion are visible around the central crystal Bragg peak. The eight first-order sidebands closest to the crystal Bragg peak are at positions  $(2 \pm \alpha\ 2 \pm \alpha\ 4 \pm \beta)$ , where  $\alpha \approx 0.055$  and

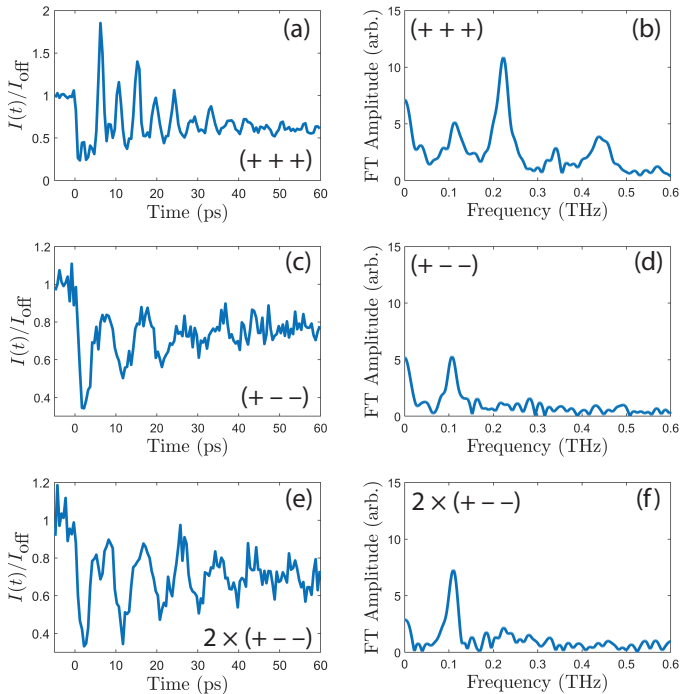


FIG. 2. Time-domain signal and Fourier spectra obtained at (a,b) the  $(2\ 2\ 4)$   $(++)$  sideband, (c,d) the  $(2\ 2\ 4)$   $(+-)$  sideband, and (e,f) the  $(2\ 2\ 4)$   $2\times(+--)$  sideband. The measured signals  $I$  are normalized by the static sideband diffraction in the absence of the pump laser pulse  $I_{\text{off}}$ . Prominent oscillations at 0.11 THz are observed at approximately the same amplitude for all peaks, whereas the amplitudes of the 0.23 and 0.46 THz modes vary significantly among the different sidebands. Prominent 0.11 THz signal is also observed in the second-order sidebands. These measurements were made during the SACLA experiment with an 800 nm pump fluence of 34 mJ/cm<sup>2</sup> and a pump polarization rotated 45° out of the plane of incidence.

$\beta \approx 0.112$  r.l.u. Also visible are some of the second-order sidebands at  $(2 \pm 2\alpha\ 2 \pm 2\alpha\ 4 \pm 2\beta)$ . For simplicity of notation, we will refer to sideband indices by their sign, e.g.  $(-+-)$  represents  $(-\alpha\ \alpha\ -\beta)$ , whereas  $2\times(-+-)$  is  $(-2\alpha\ 2\alpha\ -2\beta)$ . The corresponding labels for each of the sidebands observed are provided in Fig. 1(d). According to the structural determination [19] the CDW phase features a single wavevector with 4 possible orientational domains, which has been confirmed experimentally by the observation of single-domain x-ray diffraction [20].

Figs. 2(a,c,e) show the normalized diffracted signals  $I(t)/I_{\text{off}}$  integrated over regions of interest (ROIs) around the  $(++)$ ,  $(+-)$ , and  $2\times(+--)$  sidebands as a function of pump-probe delay, where  $I(t)$  is the recorded x-ray intensity and  $I_{\text{off}}$  is the equilibrium intensity. The data obtained at all twelve observed CDW sidebands around the  $(2\ 2\ 4)$  crystal Bragg peak is provided in the Supplemental Material [30]. As is evident from the amplitude of the Fourier transforms shown in Figs. 2(b,d,f),

there are three prominent oscillatory components at 0.11, 0.23, and 0.46 THz. The 0.11 THz signal appears at all sidebands with approximately equal normalized amplitude, while the 0.23 and 0.46 THz signals vary significantly with sideband index. For example, the  $(++)$  sideband in Fig. 2(a-b) contains all three components, while the  $(+-)$  sideband in Fig. 2(c-d) only shows the 0.11 THz mode. All three components are absent from the I422 crystal Bragg peaks [30]. The appearance of the 0.11 THz signal at all sidebands with the same relative amplitude indicates that it corresponds to a mode with a polarization that projects strongly onto the polarization of the equilibrium CDW lattice distortion, which has a primarily TA character. Additionally, the fact that the 0.11 THz signal appears at the second-order sidebands as well indicates that it is a collective mode of the CDW rather than a zone-folded acoustic phonon (in the latter case, the frequency of a linearly dispersing acoustic mode should double between  $\mathbf{q}_{\text{CDW}}$  and  $2\mathbf{q}_{\text{CDW}}$ ). Furthermore, the observed frequency is close to the TA phonon frequency at  $\mathbf{q}_{\text{CDW}}$  for the high-temperature phase, which is calculated to be 0.13 THz from measured values of the elastic constants [31]. The fact that none of the Raman-active modes soften near the transition [32, 33] indicates that there is not a dramatic general renormalization of the lattice dynamics upon crossing into the CDW phase, suggesting a valid comparison between modes above and below  $T_c$  with similar frequencies. From these considerations we identify the mode at 0.11 THz as an amplitude mode of the CDW derived primarily from the I422-phase TA phonon mode at  $\mathbf{q}_{\text{CDW}}$ .

The other two acoustic modes at  $\mathbf{q}_{\text{CDW}}$ , as determined from calculations based on experimental values of the I422-phase elastic constants [31], are a quasi-transverse acoustic (QTA) mode at a frequency of 0.20 THz and a quasi-longitudinal acoustic (QLA) mode at a frequency of 0.38 THz. The calculated frequency of the QTA mode is close to the observed 0.23 THz, and we thus assign the 0.23 THz component to the QTA mode at  $\mathbf{q}_{\text{CDW}}$ . The 0.46 THz component is likely the second harmonic of the QTA mode arising from the nonlinear dependence of the diffracted intensity on the mode amplitude [34].

Similar frequencies as those shown in Fig. 2 have been reported in optical reflectivity measurements [33]. These have been tentatively associated with the CDW phase because they disappear for  $T > T_c$ . However, from such measurements is not possible to determine the polarizations of these modes. Additionally, since none of the components in these measurements exhibit any critical temperature dependence it is not possible to distinguish the collective mode of the CDW from a folded phonon mode at  $\mathbf{q}_{\text{CDW}}$  [5, 6]. Due to the momentum resolution of our measurements we are able to make both of these determinations.

We model the 0.11 THz signal from the TA-derived amplitude mode at the  $(2\ 2\ 4)$  sidebands as a dispersive excitation of a harmonic oscillator [30, 35]. We consider a potential of the form

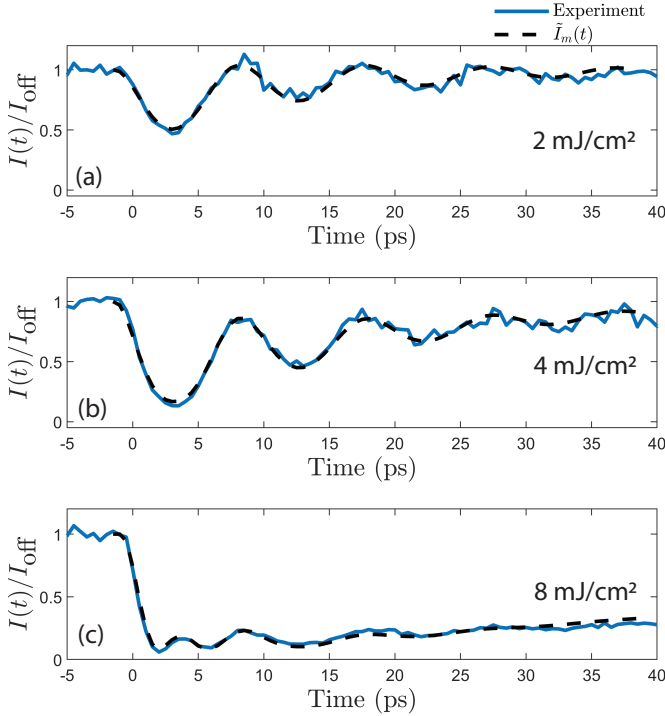


FIG. 3. Normalized signal at the (2 2 4)  $(- + -)$  sideband for pump fluences of (a) 2 mJ/cm<sup>2</sup>, (b) 4 mJ/cm<sup>2</sup>, and (c) 8 mJ/cm<sup>2</sup>, obtained during the LCLS experiment. The pump was  $p$ -polarized with a wavelength of 2  $\mu$ m. Dashed lines are the fits obtained for the model  $I_m(t)$  described in the text. For all three fluences the fitted value obtained for the restoring frequency  $\nu_0 \equiv \sqrt{c}/2\pi$  was 0.11 THz.

$$V(\xi, t) = \frac{1}{2}a[\xi - \xi_0(t)]^2 \quad (1)$$

$$\xi_0(t) \equiv 1 - \eta\Theta(t)e^{-t/\tau}$$

which yields an equation of motion given by

$$\frac{1}{c}\ddot{\xi} = -\xi + \xi_0(t) - \gamma\dot{\xi}. \quad (2)$$

In this model,  $\eta$  represents the excitation fluence,  $\tau$  is the relaxation timescale of the potential following excitation,  $c$  governs the oscillation frequency,  $\gamma$  is a phenomenological damping rate, and  $\Theta(t)$  is the Heaviside step function. We define  $\xi = 0$  as the point at which the x-ray structure factor of the mode vanishes, and  $\xi = 1$  as the equilibrium position in the CDW phase. The structure factor associated with the secondary Ta-tetramerization component of the equilibrium lattice distortion vanishes at (2 2 4) by symmetry and is thus negligibly small at the small-wavevector CDW sidebands surrounding (2 2 4) [18]. Additionally, at several of the CDW sidebands, for example  $(- + -)$ , only the 0.11 THz signal is observed with the 0.23 THz component absent. Since

the tetramerization modes and the QTA mode are all extinct at these sidebands, the only lattice component that contributes to the x-ray diffraction is the TA component corresponding to  $\xi(t)$ . Given that the diffracted intensity at a CDW sideband is proportional to the square of the amplitude of the CDW lattice distortion [34], and since only the TA component is detectable at these sidebands, the entire x-ray diffraction signal at these peaks should be proportional to  $(\xi(t))^2$ .

Using Eq. 2 we model the diffraction signal at the  $(- + -)$  sideband as  $\tilde{I}_m(t) = (\xi(t))^2 + \tilde{I}_{os}$ , where  $\tilde{I}_{os}$  is a static offset corresponding to diffraction from un-pumped material due to penetration depth mismatch. Fig. 3 shows the normalized signals observed at the  $(- + -)$  sideband for a range of excitation fluences along with the fits obtained for  $\tilde{I}_m(t)$  (details provided in the Supplemental Material [30]). We observe no dependence of the frequency  $\nu_0 \equiv \sqrt{c}/2\pi$  on the excitation fluence. The agreement shown in Fig. 3 suggests that this mode is excited through a sudden displacement of its equilibrium position (the cosine phase of the oscillation is a signature of this effect [35]), although this mode is not itself expected to couple directly to the photoexcited valence electrons given the small deformation potential expected for an acoustic mode at such a small wavevector [36]. Additionally, the lack of softening with increasing fluence further suggests that this mode is not directly affected by the photoexcited charge, since photoexcitation would change the shape of the potential and yield critical softening as the fluence approaches the melting threshold [7, 8]. In fact, at the highest fluence of 8 mJ/cm<sup>2</sup> the material is indeed excited out of the CDW phase. This can be deduced from Fig. 3(c) where at  $\sim 4$  ps the signal features a small local maximum that is not present at the lower fluences. This corresponds to  $\xi$  overshooting the origin and is a consequence of the quadratic dependence of the diffraction signal on  $\xi(t)$  [7, 8, 34]. Since  $\xi = 0$  corresponds to the equilibrium value of the TA mode in the I422 phase, the presence of this feature indicates that the CDW has been quenched by the photoexcitation. However, at this fluence we continue to observe a 0.11 THz oscillation even after the CDW has been quenched. This indicates that the 0.11 THz amplitude mode is not the mode that directly couples to the charge and drives the CDW instability, since such a mode would vanish with the CDW order at the quenching threshold. Instead, at high fluence when the I422 phase is recovered, the 0.11 THz amplitude mode simply becomes the I422-phase TA phonon and oscillates around the I422 equilibrium position of  $\xi = 0$ . The notion that the 0.11 THz amplitude mode does not directly couple to the valence charge is supported by time- and angle-resolved photoemission spectroscopy (tr-ARPES) experiments, which do not observe any oscillations in the spectral weight near the Fermi energy at this frequency following photoexcitation [37].

The lack of critical softening with increasing fluence, even past the threshold for CDW quenching, necessitates

the existence of at least one other CDW degree of freedom to mediate between this mode and the photoexcited charge. As mentioned previously, the I422 phase of TSI is predicted to be unstable to a Ta-tetramerization lattice distortion derived from a linear combination of the lowest-frequency  $B_1$  and  $B_2$  modes [22]. A prominent mode at around 2.6 THz has been observed in ultrafast reflectivity and Raman scattering below  $T_c$  [32, 33], which has been associated with a Ta-tetramerization collective mode of the CDW. These optical modes interact strongly with the charge, and through phonon-phonon coupling can induce a displacement of the TA mode.

Previous studies have speculated from the observed equilibrium structure about similar mechanisms involving interactions between the Ta-tetramerization modes and the material strain [18–20], but equilibrium measurements alone do not provide sufficient information to disentangle the active degrees of freedom of the distortion. Our time domain measurements reveal dynamics that are inconsistent with the prototypical treatment of ultrafast CDW dynamics involving a single active lattice degree of freedom. The observed 0.11 THz amplitude mode additionally has the unusual characteristics that it is derived from an acoustic rather than optical mode of the high-symmetry phase, and that it has a lower frequency than the massive phase mode observed in this material at low temperatures ( $T < 100$  K) [9]. Our findings distinguish the observed amplitude mode from an optical phason at a frequency of 0.2 THz observed recently [9] and may have implications for the axionic effects proposed for this material, which are governed by CDW collective modes [11–14].

In conclusion, we present an ultrafast x-ray study of the low energy lattice modes of  $(\text{TaSe}_4)_2\text{I}$  in the CDW phase. From the diffraction signal at different CDW sidebands we identify a mode with a frequency of 0.11 THz as an amplitude mode of the CDW derived from the dominant TA component of the CDW distortion. This mode inherits the character of the I422 TA phonon at  $\mathbf{q}_{\text{CDW}}$ , and we observe no measurable softening with pump flu-

ence even for excitations at which the lattice reaches the high-symmetry phase. These findings indicate that this mode is indirectly coupled to the valence charge through another CDW collective mode, likely associated with the secondary Ta-tetramerization component of the CDW lattice distortion. Our measurements reveal experimentally that the CDW in TSI has a composite nature involving multiple intercoupled lattice degrees of freedom, unlike conventional systems studied in the past. These results also highlight the ability of ultrafast time-domain approaches to resolve such mechanisms in systems exhibiting composite orders.

## ACKNOWLEDGMENTS

This work was primarily supported as part of the Quantum Sensing and Quantum Materials, an Energy Frontier Research Center funded by the U.S. Department of Energy (DOE), Office of Science, Basic Energy Sciences (BES) at the University of Illinois at Urbana-Champaign under Award No. DE-SC0021238 and at SLAC National Accelerator Laboratory. F.M. acknowledges support from the EPiQS program of the Gordon and Betty Moore Foundation, Grant GBMF11069. R.A.D. acknowledges support through the Bloch Postdoctoral Fellowship in Quantum Science and Engineering from the Stanford University Quantum Fundamentals, Architectures, and Machines initiative (Q-FARM), and the Marvin Chodorow Postdoctoral Fellowship from the Stanford University Department of Applied Physics. S.B. acknowledges support through the Early Postdoc Mobility Fellowship from the Swiss National Science Foundation (Grant number P2EZP2 191885). Use of the LCLS is supported by the US Department of Energy, Office of Science, Office of Basic Energy Sciences under Contract No. DE-AC02-76SF00515. X-ray measurements at BL3 of SACL A were performed with the approval of the Japan Synchrotron Radiation Research Institute (JASRI) (Proposal Nos. 2021A8037).

- 
- [1] G. Grüner, *Density Waves in Solids* (Perseus Publishing, Cambridge, MA, 1994).
  - [2] G. Grüner, The dynamics of charge-density waves, *Rev. Mod. Phys.* **60**, 1129 (1988).
  - [3] M. Bargheer, N. Zhavoronkov, M. Woerner, and T. Elsaesser, Recent progress in ultrafast x-ray diffraction, *ChemPhysChem* **7**, 783 (2006).
  - [4] R. V. Yusupov, T. Mertelj, J.-H. Chu, I. R. Fisher, and D. Mihailovic, Single-particle and collective mode couplings associated with 1- and 2-directional electronic ordering in metallic  $R\text{Te}_3$  ( $R = \text{Ho}, \text{Dy}, \text{Tb}$ ), *Phys. Rev. Lett.* **101**, 246402 (2008).
  - [5] H. Schäfer, V. V. Kabanov, M. Beyer, K. Biljakovic, and J. Demsar, Disentanglement of the electronic and lattice parts of the order parameter in a 1D charge density wave system probed by femtosecond spectroscopy, *Phys. Rev. Lett.* **105**, 066402 (2010).
  - [6] H. Schaefer, V. V. Kabanov, and J. Demsar, Collective modes in quasi-one-dimensional charge-density wave systems probed by femtosecond time-resolved optical studies, *Phys. Rev. B* **89**, 045106 (2014).
  - [7] T. Huber, S. O. Mariager, A. Ferrer, H. Schäfer, J. A. Johnson, S. Grübel, A. Lübcke, L. Huber, T. Kubacka, C. Dornes, C. Laulhe, S. Ravy, G. Ingold, P. Beaud, J. Demsar, and S. L. Johnson, Coherent structural dynamics of a prototypical charge-density-wave-to-metal transition, *Phys. Rev. Lett.* **113**, 026401 (2014).
  - [8] M. Trigo, P. Giraldo-Gallo, M. E. Kozina, T. Henighan, M. P. Jiang, H. Liu, J. N. Clark, M. Chollet, J. M. Glowina, D. Zhu, T. Katayama, D. Leuenberger, P. S. Kirchmann, I. R. Fisher, Z. X. Shen, and D. A. Reis, Coherent order parameter dynamics in  $\text{SmTe}_3$ , *Phys. Rev. B* **99**,

- 104111 (2019).
- [9] S. Kim, Y. Lv, X.-Q. Sun, C. Zhao, N. Bielinski, A. Murzabekova, K. Qu, R. A. Duncan, Q. L. D. Nguyen, M. Trigo, D. P. Shoemaker, B. Bradlyn, and F. Mahmood, Observation of a massive phason in a charge-density-wave insulator, *Nat. Mater.* **22**, 429 (2023).
- [10] P. Gressier, L. Guemas, and A. Meerschaut, Preparation and structure of ditantalum iodide octaselenide, *Ta<sub>2</sub>ISes*, *Acta Crystallogr. B* **38**, 2877 (1982).
- [11] Z. Wang and S.-C. Zhang, Chiral anomaly, charge density waves, and axion strings from Weyl semimetals, *Phys. Rev. B* **87**, 161107 (2013).
- [12] Y. You, G. Y. Cho, and T. L. Hughes, Response properties of axion insulators and Weyl semimetals driven by screw dislocations and dynamical axion strings, *Phys. Rev. B* **94**, 085102 (2016).
- [13] W. Shi, B. J. Wieder, H. L. Meyerheim, Y. Sun, Y. Zhang, Y. Li, L. Shen, Y. Qi, L. Yang, J. Jena, P. Werner, K. Koepf, S. Parkin, Y. Chen, C. Felser, B. A. Bernevig, and Z. Wang, A charge-density-wave topological semimetal, *Nat. Phys.* **17**, 381 (2021).
- [14] J. Gooth, B. Bradlyn, S. Honnali, C. Schindler, N. Kumar, J. Noky, Y. Qi, C. Shekhar, Y. Sun, Z. Wang, B. A. Bernevig, and C. Felser, Axionic charge-density wave in the Weyl semimetal (TaSe<sub>4</sub>)<sub>2</sub>I, *Nature* **575**, 315 (2019).
- [15] R. Li, J. Wang, X.-L. Qi, and S.-C. Zhang, Dynamical axion field in topological magnetic insulators, *Nat. Phys.* **6**, 284 (2010).
- [16] R. D. Peccei and H. R. Quinn, CP conservation in the presence of pseudoparticles, *Phys. Rev. Lett.* **38**, 1440 (1977).
- [17] F. Wilczek, Two applications of axion electrodynamics, *Phys. Rev. Lett.* **58**, 1799 (1987).
- [18] J. E. Lorenzo, R. Currat, P. Monceau, B. Hennion, H. Berger, and F. Levy, A neutron scattering study of the quasi-one-dimensional conductor (TaSe<sub>4</sub>)<sub>2</sub>I, *J. Phys. Condens. Matter* **10**, 5039 (1998).
- [19] S. van Smaalen, E. J. Lam, and J. Lüdecke, Structure of the charge-density wave in (TaSe<sub>4</sub>)<sub>2</sub>I, *J. Phys. Condens. Matter* **13**, 9923 (2001).
- [20] V. Favre-Nicolin, S. Bos, J. E. Lorenzo, J.-L. Hodeau, J.-F. Berar, P. Monceau, R. Currat, F. Levy, and H. Berger, Structural evidence for Ta-tetramerization displacements in the charge-density-wave compound (TaSe<sub>4</sub>)<sub>2</sub>I from x-ray anomalous diffraction, *Phys. Rev. Lett.* **87**, 015502 (2001).
- [21] P. Gressier, M. H. Whangbo, A. Meerschaut, and J. Rouxel, Electronic structures of transition-metal tetrachalcogenides (MSe<sub>4</sub>)<sub>n</sub>I (M = Nb, Ta), *Inorg. Chem.* **23**, 1221 (1984).
- [22] Y. Zhang, L.-F. Lin, A. Moreo, S. Dong, and E. Dagotto, First-principles study of the low-temperature charge density wave phase in the quasi-one-dimensional Weyl chiral compound (TaSe<sub>4</sub>)<sub>2</sub>I, *Phys. Rev. B* **101**, 174106 (2020).
- [23] M. Maki, M. Kaiser, A. Zettl, and G. Grüner, Charge density wave transport in a novel inorganic chain compound, (TaSe<sub>4</sub>)<sub>2</sub>I, *Solid State Commun.* **46**, 497 (1983).
- [24] S. Kim, R. C. McKay, N. Bielinski, C. Zhao, M.-K. Lin, J. A. Hlevyack, X. Guo, S.-K. Mo, P. Abbamonte, T.-C. Chiang, A. Schleife, D. P. Shoemaker, B. Bradlyn, and F. Mahmood, Kramers-Weyl fermions in the chiral charge density wave material (TaSe<sub>4</sub>)<sub>2</sub>I (2021), arXiv:2108.10874.
- [25] P. Emma, R. Akre, J. Arthur, R. Bionta, C. Bostedt, J. Bozek, A. Brachmann, P. Bucksbaum, R. Coffee, F.-J. Decker, Y. Ding, D. Dowell, S. Edstrom, A. Fisher, J. Frisch, S. Gilevich, J. Hastings, G. Hays, P. Hering, Z. Huang, R. Iverson, H. Loos, M. Messerschmidt, A. Miahnahri, S. Moeller, H.-D. Nuhn, G. Pile, D. Ratner, J. Rzepiela, D. Schultz, T. Smith, P. Stefan, H. Tompkins, J. Turner, J. Welch, W. White, J. Wu, G. Yocky, and J. Galayda, First lasing and operation of an ångström-wavelength free-electron laser, *Nat. Photonics* **4**, 641 (2010).
- [26] M. Chollet, R. Alonso-Mori, M. Cammarata, D. Damiani, J. Defever, J. T. Delor, Y. Feng, J. M. Glowina, J. B. Langton, S. Nelson, K. Ramsey, A. Robert, M. Sikorski, S. Song, D. Stefanescu, V. Srinivasan, D. Zhu, H. T. Lemke, and D. M. Fritz, The x-ray Pump-Probe instrument at the linac coherent light source, *J. Synchrotron Radiat.* **22**, 503 (2015).
- [27] T. Ishikawa, H. Aoyagi, T. Asaka, Y. Asano, N. Azumi, T. Bizen, H. Ego, K. Fukami, T. Fukui, Y. Furukawa, S. Goto, H. Hanaki, T. Hara, T. Hasegawa, T. Hatsui, A. Higashiyama, T. Hirono, N. Hosoda, M. Ishii, T. Inagaki, Y. Inubushi, T. Itoga, Y. Joti, M. Kago, T. Kameshima, H. Kimura, Y. Kirihara, A. Kiyomichi, T. Kobayashi, C. Kondo, T. Kudo, H. Maesaka, X. M. Maréchal, T. Masuda, S. Matsubara, T. Matsumoto, T. Matsushita, S. Matsui, M. Nagasono, N. Nariyama, H. Ohashi, T. Ohata, T. Ohshima, S. Ono, Y. Otake, C. Saji, T. Sakurai, T. Sato, K. Sawada, T. Seike, K. Shirasawa, T. Sugimoto, S. Suzuki, S. Takahashi, H. Takebe, K. Takeshita, K. Tamasaku, H. Tanaka, R. Tanaka, T. Tanaka, T. Togashi, K. Togawa, A. Tokuhisa, H. Tomizawa, K. Tono, S. Wu, M. Yabashi, M. Yamaga, A. Yamashita, K. Yanagida, C. Zhang, T. Shintake, H. Kitamura, and N. Kumagai, A compact x-ray free-electron laser emitting in the sub-ångström region, *Nat. Photonics* **6**, 540 (2012).
- [28] M. Harmand, R. Coffee, M. R. Bionta, M. Chollet, D. French, D. Zhu, D. M. Fritz, H. T. Lemke, N. Medvedev, B. Ziaja, S. Toleikis, and M. Cammarata, Achieving few-femtosecond time-sorting at hard x-ray free-electron lasers, *Nat. Photonics* **7**, 215 (2013).
- [29] T. Sato, T. Togashi, K. Ogawa, T. Katayama, Y. Inubushi, K. Tono, and M. Yabashi, Highly efficient arrival timing diagnostics for femtosecond x-ray and optical laser pulses, *Appl. Phys. Express* **8**, 012702 (2014).
- [30] See Supplemental Material at [URL] for the following: a discussion of the dispersive harmonic oscillator model used in Fig. 3 and the fitted parameter values; the ultrafast x-ray diffraction data obtained from all CDW sidebands observed in the vicinity of the (2 2 4) crystal Bragg peak; an estimate of the temperature excursion following photoexcitation; finely binned datasets showing the absence of optical modes; and measurements of the (4 2 0) crystal Bragg peak and some of its surrounding CDW sidebands. The Supplemental Material contains an additional reference [38].
- [31] M. Saint-Paul, S. Holtmeier, R. Britel, P. Monceau, R. Currat, and F. Levy, An ultrasonic and thermal expansion study of the quasi-one-dimensional compound (TaSe<sub>4</sub>)<sub>2</sub>I, *J. Phys. Condens. Matter* **8**, 2021 (1996).
- [32] S. Sugai, M. Sato, and S. Kurihara, Interphonon interactions at the charge-density-wave phase transitions in (TaSe<sub>4</sub>)<sub>2</sub>I and (NbSe<sub>4</sub>)<sub>2</sub>I, *Phys. Rev. B* **32**, 6809 (1985).
- [33] H. Schaefer, M. Koerber, A. Tomeljak, K. Biljaković,

- H. Berger, and J. Demsar, Dynamics of charge density wave order in the quasi one dimensional conductor  $(\text{TaSe}_4)_2\text{I}$  probed by femtosecond optical spectroscopy, *Eur. Phys. J. Spec. Top.* **222**, 1005 (2013).
- [34] A. W. Overhauser, Observability of charge-density waves by neutron diffraction, *Phys. Rev. B* **3**, 3173 (1971).
- [35] H. J. Zeiger, J. Vidal, T. K. Cheng, E. P. Ippen, G. Dresselhaus, and M. S. Dresselhaus, Theory for displacive excitation of coherent phonons, *Phys. Rev. B* **45**, 768 (1992).
- [36] J. Ziman, *Electrons and Phonons: The Theory of Transport Phenomena in Solids* (Oxford University Press, London, England, 1960) Chap. 5: Electron-phonon interaction.
- [37] A. Crepaldi, M. Puppini, D. Gosálbez-Martínez, L. Moreschini, F. Cilento, H. Berger, O. V. Yazyev, M. Chergui, and M. Grioni, Optically induced changes in the band structure of the weyl charge-density-wave compound  $(\text{TaSe}_4)_2\text{I}$ , *Journal of Physics: Materials* **5**, 044006 (2022).
- [38] R. Xu and T. C. Chiang, Determination of phonon dispersion relations by x-ray thermal diffuse scattering, *Z. Krist.* **220** (2005).